

Anti-disturbance State-of-Charge Estimation for Lithium-ion Batteries Using Nonlinear Extended State Observers

Shuo ZHANG, Xinghao WANG, Zifeng CHEN, and Dianxun XIAO

Abstract—In this paper, the nonlinear extended state observer (NESO) is proposed to estimate the state-of-charge (SOC) of the Lithium-ion batteries (LIBs). The NESO is designed based on the first-order equivalent circuit model (ECM) to estimate the total disturbance of the battery model and compensate them as the new extended state, which can achieve the active disturbance rejection to estimate the battery state accurately. Furthermore, the stability of the NESO is proven, and estimation performance of the observer is verified under different ambient temperatures, testing driving and different noise levels. The SOC estimation results indicate that the NESO can obtain accurate estimation values and strong robustness against different disturbances, even though all validation conditions use constant battery value of the first-order ECM. In addition, compared with other common estimation methods, the NESO exhibits a faster convergence time and more accurate estimation results.

Index Terms—Active disturbance rejection, Lithium-ion batteries (LIBs), Nonlinear extended state observer, State-of-charge (SOC)

I. INTRODUCTION

In recent years, lithium-ion batteries (LIBs) have been at the forefront of academic interest and broad application, owing to their superior characteristics including their high power and energy density, coupled with their extensive longevity [1]-[5]. The Battery Management System (BMS), an essential component within the battery application field, ensures comprehensive management and protection for batteries, thereby enhancing their reliability, durability, and safety. The State of Charge (SOC), a fundamental function within the BMS, indicates the remaining battery capacity. Accurate SOC estimation is crucial for prolonging battery lifespan and enhancing energy utilization. However, the inaccurate SOC estimation result can lead to early battery failure, decreased system efficiency, and potential safety risks. Hence, the continuous development of reliable and precise SOC estimation techniques is a key research area within the field of battery management, given its substantial impact on the practical application of battery systems.

Currently, different methods for estimating SOC have been developed and can be categorized into two types: model-free and model-based methods [6]. Model-free SOC estimation methods do not require a mathematical model of the battery but instead rely on empirical data and statistical techniques to estimate the SOC. One example of a model-free method is Coulomb counting, which estimates the SOC by integrating the current through the battery. However, this method requires accurate knowledge of the initial SOC and measurement errors

from the current sensor can accumulate during the calculation process [7]-[8]. Open circuit voltage (OCV) is another method that shows a monotonic relationship with SOC [9]. However, accurate OCV measurement requires a long relaxation time for the battery to reach its inner equilibrium, which limits its practical application in SOC estimation. To improve the accuracy of SOC estimation, advanced model-free methods such as support vector regression (SVR) [10], deep neural networks (DNNs) [11]-[12], and fuzzy logic [13] have been proposed. However, there are also some drawbacks to consider. These methods require a large amount of data to accurately train models, which can be challenging in applications where data collection and computation are limited or expensive. Additionally, these methods can become overfitted to the training data, which means they perform well on the training set but poorly on new data.

Recently, the model-based estimation method is generally considered the suitable choice for online SOC estimation due to its expected performance and reasonable computing effort [14]. Numerous LIBs models typically include two types: electrochemical and equivalent circuit model [15]. Electrochemical model is based on the electrochemical reactions and mass transfer processes inside the battery [16]-[17]. It can describe a comprehensive account of the internal dynamics of the battery. However, achieving practical applicability demands a substantial allocation of computational resources [18]. ECM is a simple model that represents the battery as an electrical circuit consisting of resistors, capacitors, and voltage sources. It is typically easier to implement and compute but provide a less detailed description of the battery compared to the electrochemical model. Currently, the ECM is often used in practical online applications since it can provide sufficient accuracy and computational efficiency while maintaining sufficient simplicity [19]. Based on the accurate battery model, different SOC estimation methods have been proposed. These methods can combine the battery model with the Coulomb integration method to recalibrate the estimated SOC, thereby reducing the SOC estimation errors. The typical model-based SOC estimation framework is shown in Fig. 1. The popular model-based estimation algorithm includes a proportional-integral observer (PIO) [20], sliding mode observer (SMO) [21], extended Kalman filter (EKF) [22]-[23], unscented Kalman filter (UKF) [24].

In [25], the PIO was employed to minimize the voltage prediction error and adjust the SOC estimation. However, the method's effectiveness can be affected by the nonlinearity of the

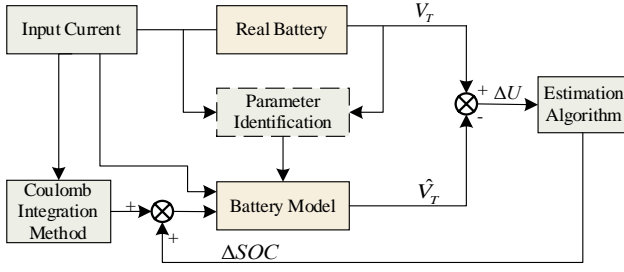


Fig. 1. Framework of model-based SOC estimation.

model and external noise. The conventional Kalman filter (KF) is a linear estimation method. To extend the application of the KF method to nonlinear battery systems, the EKF method and the UKF have been developed to estimate the SOC properly, on account of their abilities to remove the influence of measurement noise and process noise. Nevertheless, both EKF and UKF methods are complex computations due to the large number of matrix operations. In addition, the SMO scheme is also a robust method for estimating the SOC in the presence of parameter uncertainties and disturbances. However, determining the uncertainty boundaries and reducing the chattering phenomenon can be challenging.

Regarding the issues with the above methods, this paper presents a novel model-based approach for estimating the SOC using the nonlinear extended state observer (NESO). The observer is designed based on the first-order ECM to estimate the external disturbances and internal disturbances of the battery model as the new extended state and compensate them for the battery model. Compared with conventional methods, it can improve the accuracy and robustness of the SOC estimation, even though using constant battery model parameters under various operating conditions. Besides, it can reduce the convergence time effectively.

The papers are organized as follows: Section II will establish the first-order ECM and identify the parameters of the battery model using the particle swarm optimization (PSO) algorithm offline. Section III will introduce the active disturbance rejection control (ADRC) technique and design the nonlinear extended state observer for the battery model. Section IV, the robustness and accuracy of the proposed method will be verified under different testing conditions. Finally, Section V will conclude the paper.

II. BATTERY MODELING

The battery modelling is important for the battery state estimation. In this section, the PSO will be used to identify the parameters of the battery ECM.

A. First-order ECM of Battery

To keep a tradeoff between the complexity and accuracy of the battery model, this paper adopts the first-order ECM [26], as illustrated in Fig. 2. The battery dynamics are represented by a resistance-capacitance (R_1, C_1) module with an internal resistance (R_0) connected in series. The capacitor C_n represents all energy stored in the battery. $U_{soc}(t)$ represents the SOC of the battery, with 0V-1V of U_{soc} corresponding to 0%-100% of SOC [27]. The relationship between the SOC and the OCV is

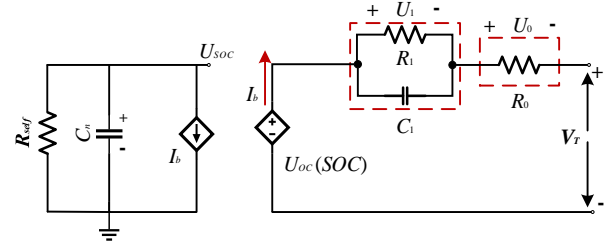


Fig. 2. First-order equivalent circuit model.

presented by the voltage-controlled voltage source, which is expressed as below:

$$U_{oc} = g(U_{soc}) \quad (1)$$

where U_{oc} denotes the OCV of the battery and $g(\cdot)$ represents the nonlinear connection between the SOC and OCV. In addition, the $U_{soc}(t)$ and $SOC(t)$ are interchangeable in the battery model [28]. R_{self} denotes the self-charging resistor. In general, it can be regarded the infinity as the self-discharging phenomenon is ignorable.

Based on Kirchhoff's laws, the dynamic electrical behavior of the first-order ECM circuit can be expressed as below:

$$\begin{cases} \dot{U}_1 = -\frac{1}{R_1 C_1} U_1 + \frac{1}{C_1} I_b \\ \dot{SOC} = -\frac{\eta_0}{3600 C_n} I_b \end{cases} \quad (2)$$

$$V_T = U_{oc}(SOC) + U_1 + U_0 \quad (3)$$

where U_1 is the terminal voltage of R_1 , I_b represents the current of the battery, V_T represents the terminal voltage of the battery, U_{oc} represents the OCV which is related to the value of SOC, and C_n represents the nominal capacity of the battery. U_0 is the

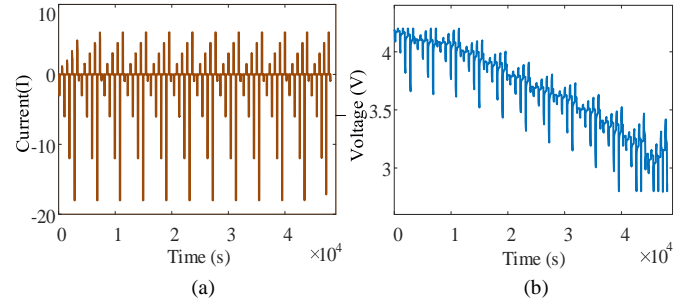


Fig. 3. The HPPC driving test of the battery. (a) Current of HPPC test. (b) Voltage of HPPC test.

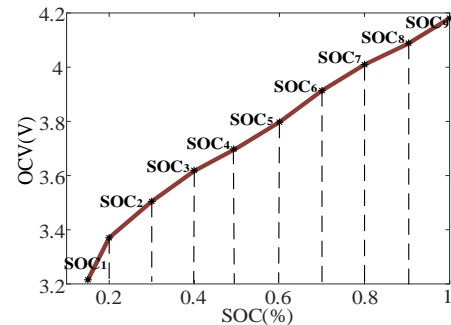


Fig. 4. SOC-OCV relationship curve.

voltage drop on the resistance R_0 . η_0 denotes the coefficient of Coulomb.

B. Offline Parameters Identification

The offline parameter identification of battery models is a common approach for the ECM. The PSO is utilized in offline parameter identification, offering advantages such as fewer parameters, faster convergence, and simpler implementation [29]. In this study, the parameters of the first-order ECM are identified offline using the PSO algorithm.

In the parameter identification and state estimation of the LIBs, the precise relationship between SOC and OCV is an essential process for accurately estimating the SOC of battery [31]. The relationship is typically non-linear and depends on factors. In general, as the SOC decreases, the OCV will also decrease. This paper gets the relationship between them through the Hybrid Pulse Power Characterization (HPPC) test, as shown in Table I. The test current and voltage of the battery is shown in Fig. 3 under the HPPC test.

Within the SOC range depicted in Fig. 4, the nonlinear correlation between OCV and SOC can be approximated as a group of linear sections. Hence, the piecewise linearization method is utilized to represent OCV as a linear function of SOC, as shown in equation (4).

$$U_{oc}(SOC) = m_i SOC + b_i \quad (4)$$

where the m_i , b_i ($i=1-9$) are two coefficients in the equation (4). The approximation parameters of the relationship between SOC and OCV are listed in Table I.

In this study, the PSO algorithm is employed for offline parameter identification of the battery model under the Urban Dynamometer Driving Schedule (UDDS) test at 25°C. The cost function is the error between the actual voltage and the estimated voltage, as shown in equation (5).

$$\min(F), \text{ where } F = \sum_{i=1}^N |V_T - \hat{V}_T| \quad (5)$$

where N is the total number of the sampling points, \hat{V}_T denotes the estimation of the terminal voltage.

In Fig. 6(a), the estimated voltage results are compared with the actual voltage. The figure demonstrates that the model-calculated terminal voltage closely aligns with the measured terminal voltage. However, some discrepancies still exist between the actual and calculated voltage due to battery model uncertainties and external disturbance. The model error of the parameter identification is about $\pm 5\%$ band, as shown in Fig. 6(b).

TABLE I
THE RELATIONSHIP BETWEEN SOC AND OCV

Relationship between SOC and OCV			
SOC _i (%)	0.15-0.2	0.2-0.3	0.3-0.4
m_i	3.101	1.341	1.124
b_i	2.750	3.102	3.167
SOC _i (%)	0.4-0.5	0.5-0.6	0.6-0.7
m_i	0.841	0.959	0.753
b_i	3.281	3.242	3.406
SOC _i (%)	0.7-0.8	0.8-0.9	0.9-1.0
m_i	0.959	0.957	1.166
b_i	3.221	3.222	3.097

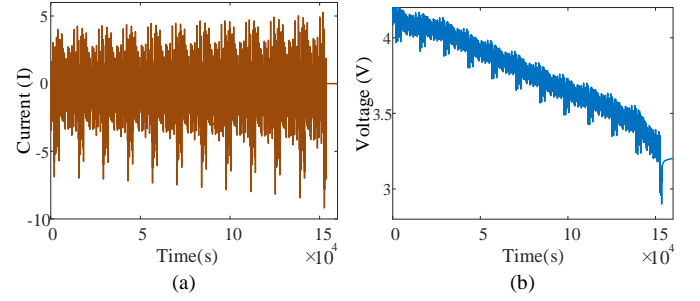


Fig. 5. The UDDS driving test of the battery. (a) Current of the UDDS test. (b) Voltage of the UDDS test.

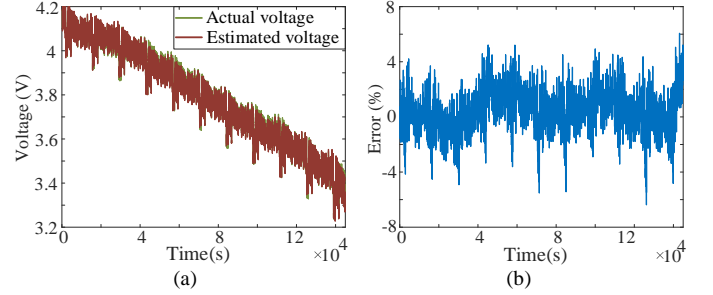


Fig. 6. The optimization result using PSO. (a) Actual and estimated voltage. (b) Voltage estimation error.

The parameter identification results of the first-order ECM are $R_0=0.02109\Omega$, $R_1=0.02711\Omega$, and $C_1=1011F$. Although the simple RC model generally captures the dynamic characteristics of the LIBs, the modelling errors persist. In Section III, the NESO will be designed to estimate the total perturbation of the battery model as the new extended state, aiming to reduce battery errors and improve estimation accuracy.

III. NESO FOR SOC ESTIMATION

In this section, the NESO is designed to estimate the SOC of the LIBs, which can effectively improve the accuracy and robustness of estimation results.

A. Introduction of ADRC and ESO

The ADRC is an approach introduced by Professor Han, which has gained widespread use in various industrial applications due to its robustness and effectiveness in addressing model uncertainties and disturbances [32]. It consists of three components, including Tracking Differentiator (TD), Extended State Observer (ESO), and Nonlinear State Error Feedback (NLSEF). The primary function of the TD is to deliver a precise and smooth approximation of the input signal's derivative. Meanwhile, the ESO aims to assess the system's state and disturbance, allowing control systems to better counteract disturbances and enhance both system performance and robustness. Lastly, the role of the NLSEF is to supply a feedback control law based on the estimated states and the desired reference values.

The diagram of the entire ADRC is shown in Fig. 7, where z_i ($i=1-n$) denote the estimated values of the system state and z_{n+1} denotes the total disturbance of the system. v denotes the reference input, v_1 denotes the transition process of reference input, v_n is the differential signal of each order of v_1 , u_0 denotes

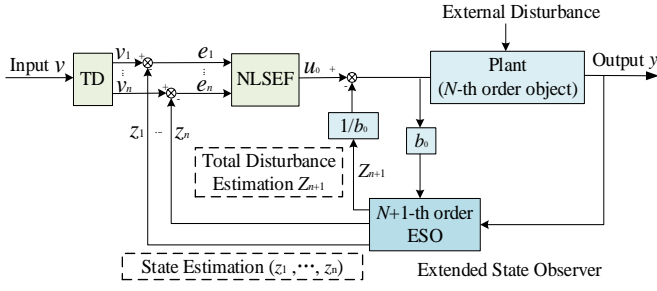


Fig. 7. Diagram of the ADRC.

the control signal, and e_i ($i=1-n$) denote system state errors. D is the external disturbance. The ESO constitutes a crucial component of the ADRC system, enabling the estimation of both system states and total disturbances. By compensating for the effects of system disturbances, the ESO enhances system performance. Moreover, it facilitates efficient state estimation without the need for an accurate system model. The ESO operates on the principle of the extended state, which encompasses both system states and total system disturbances.

By incorporating the system total disturbances into the state vector, the ESO can estimate them alongside the system states, allowing for real-time disturbance rejection. Considering the n -th order non-linear system:

$$y^{(n)}(t) = f(y^{(n-1)}(t), \dots, y(t), d(t)) + b \cdot u(t) \quad (6)$$

where $d(t)$ denotes the external disturbance, $y(t)$ and $u(t)$ denote the output and input signal, respectively. $f(y^{(n-1)}(t), \dots, y(t), d(t))$ denotes the dynamic characteristic of system, which may be the non-linear and time-varying value. In the ESO, it is regarded as the total disturbance of the system, which is observed as the new extended state. Then, the new state space of system can be expressed as below.

$$\begin{cases} \dot{z}_1 = z_2 \\ \vdots \\ \dot{z}_{n-1} = z_n \\ \dot{z}_n = z_{n+1} + b \cdot u \\ \dot{z}_{n+1} = G(d, w) \\ y = z_1 \end{cases} \quad (7)$$

with $z=[z_1, z_2 \dots z_{n+1}]^T$. The equation (7) is the new extended system of (6) as the total disturbance $f(y^{(n-1)}(t), \dots, y(t), d(t))$ is now taken as the extended state z_{n+1} . Therefore, the $N+1$ -th order ESO system can be constructed based on the original N -th order system.

$$\begin{cases} e = z_1 - \hat{z}_1 \\ \dot{\hat{z}}_1 = \hat{z}_2 + k_1 \text{fal}(e, \alpha, \delta) \\ \vdots \\ \dot{\hat{z}}_{n-1} = \hat{z}_n + k_{n-1} \text{fal}(e, \alpha, \delta) \\ \dot{\hat{z}}_n = \hat{z}_{n+1} + k_n \text{fal}(e, \alpha, \delta) + bu \\ \dot{\hat{z}}_{n+1} = k_{n+1} \text{fal}(e, \alpha, \delta) \end{cases} \quad (8)$$

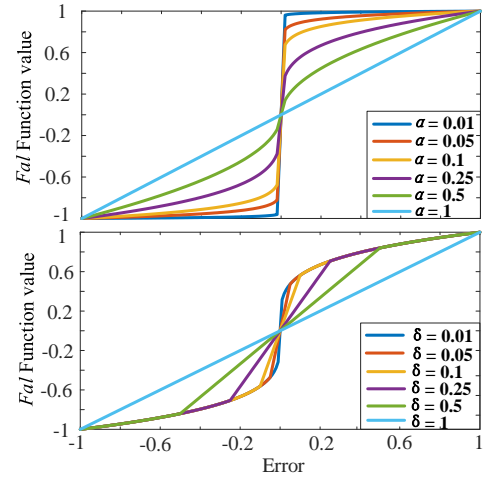


Fig. 8. Diagram of the fal function under different parameters.

where e denotes the difference between the estimated value and the actual value, \hat{z}_n denotes the estimation value of the z_n , and the constant observer gain k_i , which needs to be tuned, satisfies $k_i > 0$. ($i=1, 2, \dots, n, n+1$).

The NESO employs a nonlinear function, $\text{fal}(\cdot)$, to enhance its estimation performance, as shown in (9).

$$\text{fal}(e, \alpha, \delta) = \begin{cases} |e|^\alpha \text{sign}(e) & |e| > \delta \\ \frac{e}{\delta^{1-\alpha}} & |e| \leq \delta \end{cases} \quad (9)$$

In the nonlinear fal function, $\alpha \leq 1$ and $\delta > 0$ are important parameters of the nonlinear function due to the characteristic of the great convergence. δ is inversely proportional to the slope of the linear segment of the fal function. When $|e| \leq \delta$, the extended state observer works in the linear region to avoid high-frequency oscillations. When $|e| > \delta$, the observer works in the nonlinear region. α affects the size of the fal function.

Fig. 7(a) shows the fal function graphs when the linear interval $\delta=0.2$, α takes values of 0.01, 0.05, 0.1, 0.25, 0.5, 0.1 respectively. Fig. 7(b) shows the fal function graphs when the linear interval $\delta=0.01, 0.05, 0.1, 0.5, 0.5, 1$, respectively. It can be observed that the value of α determines the linearity of the fal function, with a smaller value resulting in a stronger nonlinearity; while the value of δ determines the linear interval of the function, with a larger value resulting in a larger linear interval.

B. SOC Estimation Using the NESO

For the battery model, the dynamic state equation of the battery can be expressed as follows based on equations (1), (2).

$$\begin{cases} \dot{x}_1 = -a_1 x_1 + a_1 U_{oc}(x_2) + b_1 I \\ \dot{x}_2 = a_2 x_1 - a_2 U_{oc}(x_2) - a_2 x_3 \\ \dot{x}_3 = -a_1 x_3 + b_2 I \end{cases} \quad (10)$$

where $a_1=1/R_1 C_1$, $a_2=1/R_0 C_n$, $b_1=((1/C_n) + (1/R_0) + (R_0/R_1 C_1))$, $b_2=1/C_1$, $x_1=V_T$, $x_2=SOC$, $x_3=U_1$. And $\dot{x}_1, \dot{x}_2, \dot{x}_3$ denote the derivation of the x_1, x_2, x_3 . However, the battery is a strong non-linear and time-varying system due to internal complex

chemical reactions. Therefore, the dynamic state equation (10) cannot describe the battery characteristics well. Considering the external and internal disturbance for the battery model, it should be expressed as shown below:

$$\begin{cases} \dot{x}_1 = -a_1 x_1 + a_1 U_{oc}(x_2) + b_1 I + x_4 \\ \dot{x}_2 = a_2 x_1 - a_2 U_{oc}(x_2) - a_2 x_3 \\ \dot{x}_3 = -a_1 x_3 + b_2 I \\ \dot{x}_4 = w(t) \end{cases} \quad (11)$$

where $w(t)$ denotes the total disturbance of the battery model including the battery model uncertainties, the aging capacity variation, the sensor noise, and so forth. For battery model (11), the accurate estimation of the total disturbances in the battery model is the key to achieving the accurate SOC estimation. This paper employs the NESO to accurately estimate the total disturbance of the battery model and compensate them as the extended state. The NESO for the state equation in (11) is designed as below.

$$\begin{cases} \dot{\hat{x}}_1 = -a_1 \hat{x}_1 + a_1 V_{oc} \hat{x}_2 + b_1 I + \hat{x}_4 - k_1 fal(e_1, \alpha, \delta) \\ \dot{\hat{x}}_2 = a_2 \hat{x}_1 - a_2 V_{oc} \hat{x}_2 - a_2 \hat{x}_3 - k_2 fal(e_1, \alpha, \delta) \\ \dot{\hat{x}}_3 = \hat{x}_3 - a_1 \hat{x}_3 + b_2 I - k_3 fal(e_1, \alpha, \delta) \\ \dot{\hat{x}}_4 = -k_4 fal(e_1, \alpha, \delta) \\ e_1 = \hat{x}_1 - x_1 \end{cases} \quad (12)$$

where e denotes the error between the estimated terminal and the actual voltage. k_1, k_2, k_3 , and k_4 denote the adjustable gain of the NESO algorithm. The \hat{x}_4 denotes the total disturbance of the battery model. When the system reaches stability, the estimated extended state x_4 can be expressed as below.

$$\hat{x}_4 = -\int k_4 fal(e_1, \alpha, \delta) \quad (13)$$

To better adapt to computer programming, equation (12) is Eulerian discretized to obtain the expression as shown in (14).

$$\begin{cases} \hat{x}_1(k+1) = \hat{x}_1(k) + T_s [-a_1 \hat{x}_1(k) + a_1 V_{oc}(\hat{x}_2(k)) + b_1 I(k) \\ \quad + \hat{x}_4(k) - k_1 fal(e_1(k), \alpha, \delta)] \\ \hat{x}_2(k+1) = \hat{x}_2(k) + T_s [a_2 \hat{x}_1(k) - a_2 V_{oc}(\hat{x}_2(k)) - a_2 \hat{x}_3(k) \\ \quad - k_2 fal(e_1(k), \alpha, \delta)] \\ \hat{x}_3(k+1) = \hat{x}_3(k) + T_s [-a_1 \hat{x}_3(k) + b_2 I(k) \\ \quad - k_3 fal(e_1(k), \alpha, \delta)] \\ \hat{x}_4(k+1) = \hat{x}_4(k) + T_s [-k_4 fal(e_1(k), \alpha, \delta)] \\ e_1(k) = \hat{x}_1(k) - x_1(k) \end{cases} \quad (14)$$

where T_s represents the sampling time, namely, 1s. The total diagram of the SOC and SOE estimation using NESO is shown in Fig. 11.

C. Stability Analysis for the NESO

Define the $F=fal(e_1)/e_1$. Then, $fal(e_1)=F \cdot e_1$. Thus, fal can be seen as the linear function e with the varying gain. In addition, define the $e_1=\hat{x}_1-x_1$, $e_2=\hat{x}_2-x_2$, $e_3=\hat{x}_3-x_3$, $e_4=\hat{x}_4-x_4$, and subtracting

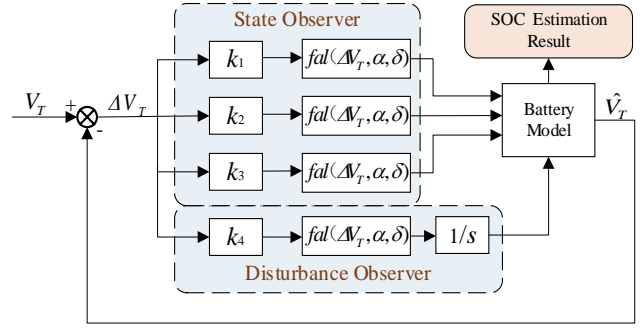


Fig. 9. Diagram of SOC estimation using the NESO.

(11) from (12) yield the 4-th order error dynamic equations as (15) and (16).

$$\begin{cases} \dot{e}_1 = (-a_1 - k_1 F)e_1 + a_1 m_1 e_2 + e_4 \\ \dot{e}_2 = (a_2 - k_2 F)e_1 - a_2 m_1 e_2 - a_2 e_3 \\ \dot{e}_3 = -k_3 F e_1 - a_1 e_3 \\ \dot{e}_4 = -k_4 F e_1 - w(t) \end{cases} \quad (15)$$

$$V_{oc}(x_2) - V_{oc}(\hat{x}_2) = m_1 e_2 \quad (16)$$

where $\dot{e}_1, \dot{e}_2, \dot{e}_3, \dot{e}_4$ denote the derivation of the e_1, e_2, e_3, e_4 . The problem formulation is that for the bounded and uncertain function $w(t)$, how to set the coefficients of fal function, k_1, k_2, k_3, k_4 to force the error e_1, e_2, e_3 , and e_4 to converge zero.

The error state equation can be expressed as below based on (15).

$$\dot{e} = -A(e) \cdot e \quad (19)$$

where $e = [e_1, e_2, e_3, e_4]^T$,

$$A(e) = \begin{bmatrix} a_1 + k_1 F & -a_1 m_1 & 0 & -1 \\ -a_2 + k_2 F & a_2 m_1 & a_2 & 0 \\ k_3 F & 0 & a_1 & 0 \\ k_4 F & 0 & 0 & 0 \end{bmatrix} \quad (20)$$

In (20), apparently F is larger than zero and has the boundary. The relationship between the positive definiteness of the sequential principal minors and the stability of the state equation is as follows: if all the sequential principal minors of the error matrix of the state equation are positive, then the system is stable. The positive definiteness of the sequential principal minors ensures that all the real parts of the eigenvalues of the system's transfer matrix are negative, thus causing the state of system to converge to stability after a certain period. Based on the theorem, If the condition satisfied in (21), the system can be stable.

$$\begin{cases} a_1 + k_1 F > 0 \\ a_2 F k_1 m_1 + a_1 F k_2 m_1 > 0 \\ a_1 a_2 F k_1 m_1 + a_1^2 F k_2 m_1 - a_1 a_2 F k_3 m_1 > 0 \\ a_1 a_2 F k_4 m_1 > 0 \end{cases} \quad (21)$$

Based on the equation (21), the solution of the observer gain is shown as below.

$$\begin{cases} a_2 k_1 + a_1 k_2 - a_2 k_3 > 0 \\ k_4 > 0 \end{cases} \quad (22)$$

IV. RESULTS AND DISCUSSION

A. Experiment Setup

In this section, the feasibility and advantages of the proposed method are verified. The verification process encompasses two distinct SOC scenarios: known initial SOC and unknown initial SOC. Additionally, the algorithm's robustness and accuracy undergo extensive testing across a range of temperature conditions, different testing driving, and different sensor noise levels. The estimation results illustrate that the proposed method has better performance compared to conventional algorithms.

The initial dataset can be accessed from the public dataset conducted at McMaster University [37]. Table II provides detailed specifications of the tested battery and adjustable parameters of the NESO. NESO's performance is evaluated using four metrics: maximum error (MAXE), root mean square error (RMSE), mean absolute error (MAE), and convergence time. *RMSE* is employed to assess performance in the regression models, and the formula is presented as below.

$$RMSE = \frac{\sum_{i=1}^n (\hat{y}_i - y_i)^2}{n} \quad (25)$$

The *MAE* is also a commonly employed performance metric in regression models. The formula for it is presented as below.

$$MAE = \frac{\sum_{i=1}^n |\hat{y}_i - y_i|}{n} \quad (26)$$

B. Estimation Result under the Accurate or Inaccurate SOC

In the first scenario, the initial SOC is known for the NESO. The SOC estimation results with the UDDS testing cycle at 25°C are depicted in Fig. 12. The figure illustrates that the estimated SOC rapidly converges to the reference and maintains accurate tracking within the $\pm 3\%$ bound. In the second scenario, where the initial SOC for the NESO is assumed to be unknown, the estimation results are presented in Fig. 13. Additional estimation assessment metrics are provided in Table III. These metrics indicate that the NESO can effectively compensate for the initial SOC error and uncertainty in the battery model, ensuring that errors remain within a small range.

TABLE II
PARAMETERS OF THE TESTED BATTERY AND THE NESO ALGORITHM

Parameters	Values
Type/Material	LiNiMnCoO ₂ +SiO ₂
Nominal Voltage	3.6V
Nominal Capacity	3Ah
Energy Density	240Wh/Kg
Cut-off Discharge Voltage	2V
Cut-off Charge Voltage	4.2V
α	0.5
δ	0.02
k_1	0.65
k_2	0.012
k_3	0.0001
k_4	0.0005

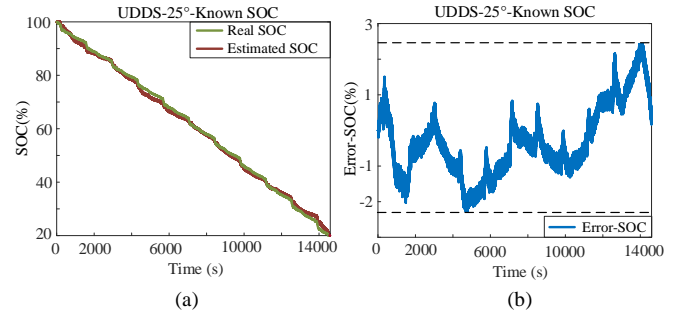


Fig. 12. SOC estimation results using the NESO at 25 °C with UDDS testing driving. (a) Actual and Estimated SOC. (b) SOC estimation error.

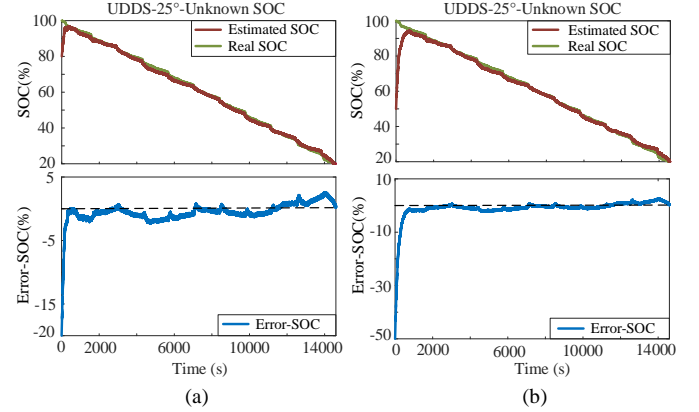


Fig. 13. SOC estimation results using the NESO at 25 °C with UDDS testing driving. (a) Estimation results under 80% initial SOC. (b) Estimation results under 70% initial SOC.

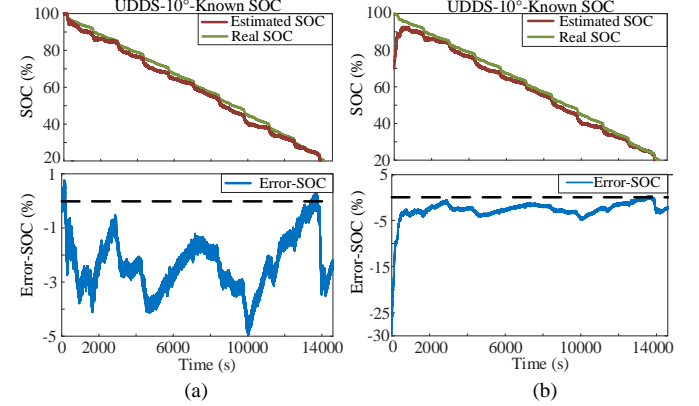


Fig. 14. SOC estimation results using the NESO at 10 °C with UDDS testing driving. (a) Estimation results under known SOC. (b) Estimation results under 70% initial SOC.

C. SOC Estimation under Different Temperature Tests

The temperature is the crucial factor affecting the accuracy of parameter identification. To verify the robustness of the NESO against temperature change, the algorithm is evaluated at 10°C and 40°C. The result is shown in Fig. 14 and Fig. 15. Under the known initial SOC, the maximum error of SOC estimation is bounded within the $\pm 5\%$. Under the unknown initial SOC (set the 70% initial SOC), the SOC estimation results can converge the real SOC faster. It indicates the proposed method is robust under different ambient temperatures, even though using one set RC value of the battery model. Notably, the robustness and accuracy of NESO at 10°C is weaker than 40°C and 25°C. The reason is that the modelling

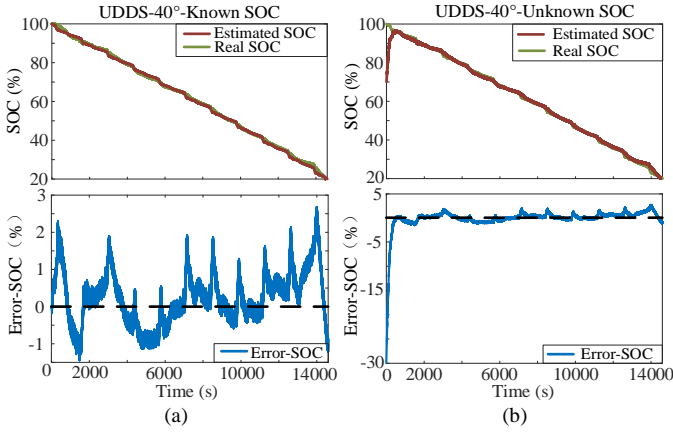


Fig. 15. SOC estimation results using the NESO at 40 °C with UDDS testing driving. (a) Estimation results under known SOC. (b) Estimation results under 70% initial SOC.

parameters of the battery have changed considerably at low temperatures, but good accuracy is still guaranteed.

D. SOC Estimation under Different Working Conditions

The estimation results are shown in the Fig. 16 and Fig. 17 with the UDDS, LA92, and US06 testing driving. Under the known initial SOC, the maximum error of the battery can be bounded within $\pm 3.5\%$. Under the unknown initial SOC, the SOC estimation can rapidly converge the real SOC and get accurate estimation results with the smaller RMSE and MAE, as listed in Table III. The results indicate that the proposed method can keep great robustness under different working conditions.

E. Compared with Other SOC Estimation Methods.

To further verify the estimation performance using the NESO, the comparison between the proposed method and other common methods including the PIO, SMO, EKF, and UKF. The estimation results are shown from Fig. 18 and Fig. 19, and Table IV. In terms of convergence time (converge to the 5% estimation error), the proposed method can converge faster than other methods with only 145s. In terms of the estimation accuracy of the SOC, the RMSE and MAE of the proposed method are smaller than other common methods under an unknown initial SOC at 25°C.

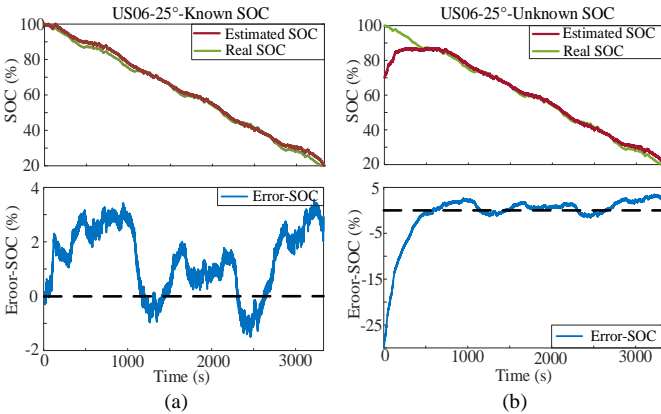


Fig. 16. SOC estimation results using the NESO at 25°C with US06 testing driving. (a) Estimation results under known SOC. (b) Estimation results under 70% initial SOC.

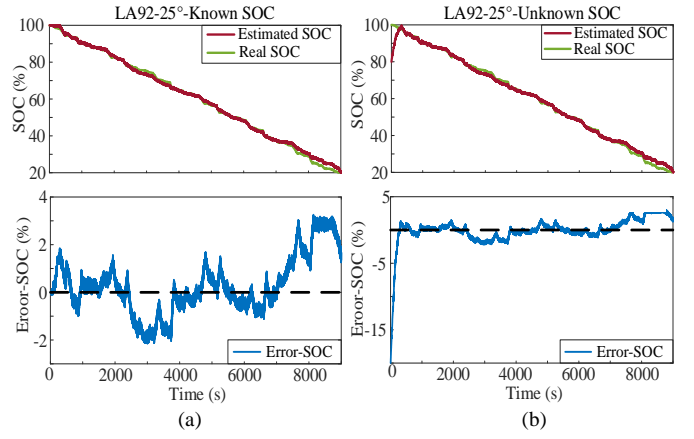


Fig. 17. SOC estimation results using the NESO at 25°C with LA92 testing driving. (a) Estimation results under known SOC. (b) Estimation results under 80% initial SOC.

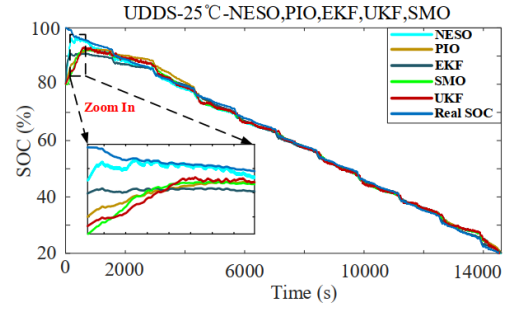


Fig. 18. SOC estimation results using different methods under 80% initial SOC.

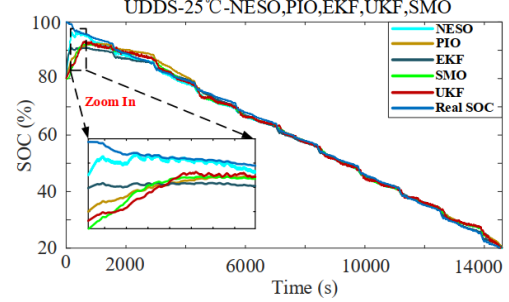


Fig. 19. SOC estimation error using different methods under 80% initial SOC.

TABLE III
COMPARISON RESULTS UNDER DIFFERENT TESTING DRIVING

SOC Estimation	Known SOC	Unknown SOC (80% SOC)	
	MAXE	MAE	RMSE
UDDS	2.62%	1.04%	1.69%
US06	3.55%	1.55%	1.83%
LA92	3.25%	1.13%	2.09%

TABLE IV
COMPARISON RESULTS USING DIFFERENT ESTIMATION METHODS

Methods	Convergence Time	RMSE	MAE
Proposed	145s	1.69%	1.04%
PIO	528s	2.58%	1.44%
EKF	471s	2.81%	1.42%
UKF	603s	2.10%	1.15%
SMO	500s	2.74%	1.43%

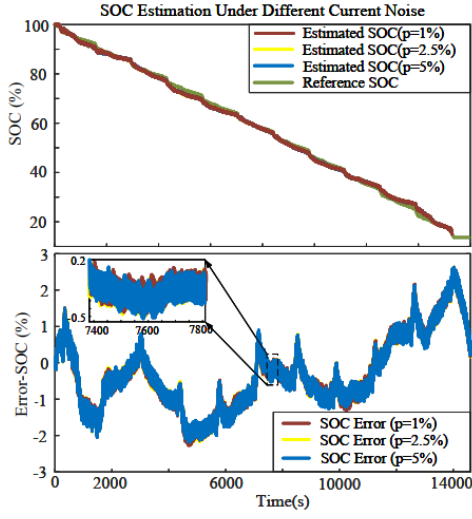


Fig. 20. SOC estimation results under different current noise levels

F. SOC Estimation under Different Noise Tests

In industrial applications, the battery management system often encounters elevated levels of noise in voltage and current sensors compared to laboratory testing. To assess the effectiveness of the proposed method in the presence of inaccurate voltage and current values, random noise (normally distributed) was introduced to the original signal. The noise possesses an average value of zero, and the standard deviation can be calculated as follows.

$$\sigma = \frac{1}{3} p I_{b, \max} \quad (28)$$

where σ denotes standard deviation of the random noise, p is a proportionality factor, and $I_{b, \max}$ is the maximum voltage or current of the battery. To verify the robustness of the proposed method against the current sensor noise at different levels. The p can be set as 1%, 2.5%, and 5%, and the SOC estimation results are shown in Fig. 20 and Table V. The maximum error for the SOC estimation results can be constrained within $\pm 3\%$, and the value of RMSE can remain stable with the current noise change. It indicates that the proposed method has strong robustness against current sensor noise.

To verify the robustness of the proposed method against the voltage sensor noise, the p can be set as 1%, 2.5%, and 5%. The SOC estimation results are shown in Fig. 21 and Table V. The maximum error for the SOC estimation results can be constrained within $\pm 5\%$, and the RMSE value remains stable even with changes in voltage sensor noise. It indicates that the proposed method has strong robustness against voltage sensor noise.

TABLE V
ESTIMATION RESULTS UNDER DIFFERENT NOISE LEVELS

Factor p (Current)	1%	2.5%	5%
MAXE	2.63%	2.63%	2.63%
RMSE	1.06%	1.05%	1.06%
Factor p (Voltage)	1%	2.5%	5%
MAXE	2.66%	2.84%	4.90%
RMSE	1.08%	1.19%	1.54%

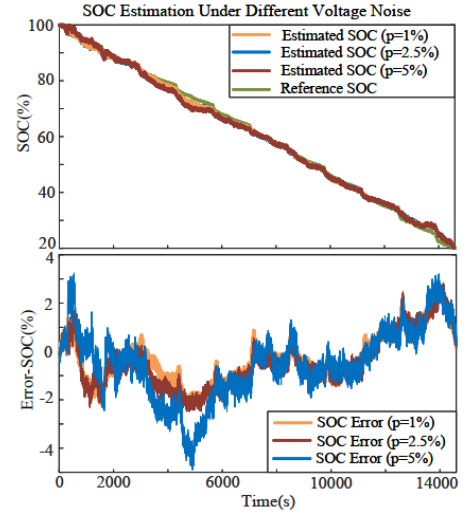


Fig. 21. SOC estimation results under different voltage noise levels

V. CONCLUSION

In this paper, a NESO is designed to estimate the SOC of LIBs, which can estimate the total disturbance of the battery model as the new extended state and compensate for them to achieve more accurate estimation results. The stability of NESO has been demonstrated, and the estimation performance of the proposed has been validated across diverse testing conditions. The obtained results indicate that the NESO has strong robustness against disturbances and can achieve more accurate state estimation of LIBs under various ambient temperatures, driving cycles and different level noises. Furthermore, in comparison to other commonly used methods, NESO demonstrates better performance in terms of convergence time and estimation accuracy.

VI. REFERENCES

- [1] Xiao *et al.*, "Reduced-Coupling Coestimation of SOC and SOH for Lithium-Ion Batteries Based on Convex Optimization," *IEEE Trans. Power Electron.*, vol. 35, no. 11, pp. 12332–12346, Nov. 2020.
- [2] S. Fu *et al.*, "Data-driven capacity estimation for lithium-ion batteries with feature matching-based transfer learning method," *Applied Energy*, vol. 353, pp. 121991, Jan. 2024.
- [3] S. Tao *et al.*, "Battery Cross-Operation-Condition Lifetime Prediction via Interpretable Feature Engineering Assisted Adaptive Machine Learning," *ACS Energy Lett.*, vol. 8, no. 8, pp. 3269–3279, Aug. 2023.
- [4] S. Zhang, X. Wang, C. Li, and D. Xiao, "Robust State of Charge Estimation for Battery with Self-Adaptive Super Twisting Sliding Mode Observer," in *IECON 2023- 49th Annual Conference of the IEEE Industrial Electronics Society*, Singapore, Singapore: IEEE, Oct. 2023.
- [5] Z. Chen *et al.*, "General-Purpose High-Speed Position-Sensorless Control of Switched Reluctance Motors Using Single-Phase Adaptive Observer," *IEEE Trans. Transp. Electric.*, pp. 1–1, 2023.
- [6] J. Meng *et al.*, "An Overview and Comparison of Online Implementable SOC Estimation Methods for Lithium-Ion Battery," *IEEE Trans. on Ind. Applicat.*, vol. 54, no. 2, pp. 1583–1591, Mar. 2018.

- [7] X. Tang, Y. Wang, and Z. Chen, "A method for state-of-charge estimation of LiFePO₄ batteries based on a dual-circuit state observer," *Journal of Power Sources*, vol. 296, pp. 23–29, Nov. 2015.
- [8] A. Nugroho, E. Rijanto, F. D. Wijaya, and P. Nugroho, "Battery state of charge estimation by using a combination of Coulomb Counting and dynamic model with adjusted gain," in *2015 International Conference on Sustainable Energy Engineering and Application (ICSEEA)*, Bandung, Indonesia: IEEE, pp. 54–58, Oct. 2015.
- [9] L. Lu, X. Han, J. Li, J. Hua, and M. Ouyang, "A review on the key issues for lithium-ion battery management in electric vehicles," *Journal of Power Sources*, vol. 226, pp. 272–288, Mar. 2013.
- [10] J. C. Álvarez Antón, P. J. García Nieto, C. Blanco Viejo, and J. A. Vilán Vilán, "Support Vector Machines Used to Estimate the Battery State of Charge," *IEEE Trans. Power Electron.*, vol. 28, no. 12, pp. 5919–5926, Dec. 2013.
- [11] M. Gholizadeh and F. R. Salmasi, "Estimation of State of Charge, Unknown Nonlinearities, and State of Health of a Lithium-Ion Battery Based on a Comprehensive Unobservable Model," *IEEE Transactions on Industrial Electronics*, vol. 61, no. 3, pp. 1335–1344, March 2014.
- [12] A. A. Hussein, "Adaptive Artificial Neural Network-Based Models for Instantaneous Power Estimation Enhancement in Electric Vehicles' Lilon Batteries," *IEEE Transactions on Industry Applications*, vol. 55, no. 1, pp. 840–849, Jan.-Feb. 2019.
- [13] H. Dastres, A. Mohammadi and M. Shamekhi, "A Neural Network Based Adaptive Sliding Mode Controller for Pitch Angle Control of a Wind Turbine," *2020 11th Power Electronics, Drive Systems, and Technologies Conference (PEDSTC)*, pp. 1–6, 2020.
- [14] J. Meng, D.-I. Stroe, M. Ricco, G. Luo, and R. Teodorescu, "A simplified model-based state-of-charge estimation approach for lithium-ion battery with the dynamic linear model," *IEEE Trans. Ind. Electron.*, vol. 66, no. 10, pp. 7717–7727, Oct. 2019.
- [15] K. Liu, X. Hu, Z. Wei, Y. Li, and Y. Jiang, "Modified Gaussian process regression models for cyclic capacity prediction of lithium-ion batteries," *IEEE Trans. Transport. Electrific.*, vol. 5, no. 4, pp. 1225–1236, Dec. 2019.
- [16] M. Xu, R. Wang, P. Zhao, and X. Wang, "Fast charging optimization for lithium-ion batteries based on dynamic programming algorithm and electrochemical-thermal-capacity fade coupled model," *J. Power Sources*, vol. 438, Art. no. 227015, Oct. 2019.
- [17] H. Li et al., "State of charge estimation for lithium-ion battery using an electrochemical model based on electrical double layer effect," *Electrochim. Acta*, vol. 326, Art. no. 134966, Dec. 2019.
- [18] X. Hu, S. Li, and H. Peng, "A comparative study of equivalent circuit models for li-ion batteries," *J. Power Sources*, vol. 198, pp. 359–367, Jan. 2012.
- [19] X. Bian, Z. Wei, J. He, F. Yan, and L. Liu, "A Two-Step Parameter Optimization Method for Low-Order Model-Based State-of-Charge Estimation," *IEEE Trans. Transp. Electrific.*, vol. 7, no. 2, pp. 399–409, Jun. 2021.
- [20] J. Xu, C. C. Mi, B. Cao, J. Deng, Z. Chen and S. Li, "The State of Charge Estimation of Lithium-Ion Batteries Based on a Proportional-Integral Observer," *IEEE Transactions on Vehicular Technology*, vol. 63, no. 4, pp. 1614–1621, May 2014.
- [21] J. Du, Z. Liu, Y. Wang, and C. Wen, "An adaptive sliding mode observer for lithium-ion battery state of charge and state of health estimation in electric vehicles," *Control Engineering Practice*, vol. 54, pp. 81–90, Sep. 2016.
- [22] S. Fu et al., "State of charge estimation of lithium-ion phosphate battery based on weighted multi-innovation cubature Kalman filter," *Journal of Energy Storage*, vol. 50, p. 104175, Jun. 2022.
- [23] Y. Shen, "Adaptive extended Kalman filter based state of charge determination for lithium-ion batteries," *Electrochimica Acta*, vol. 283, pp. 1432–1440, Sep. 2018.
- [24] Y. Tian, B. Xia, W. Sun, Z. Xu, and W. Zheng, "A modified model-based state of charge estimation of power lithium-ion batteries using unscented Kalman filter," *Journal of Power Sources*, vol. 270, pp. 619–626, Dec. 2014.
- [25] Quan Ouyang, J. Chen, and Keyou You, "State of charge estimation of lithium-ion batteries with unknown model parameters," in *2016 American Control Conference (ACC)*, Boston, MA, USA: IEEE, pp. 4012–4017, Jul. 2016.
- [26] M. Chen and G. A. Rincon-Mora, "Accurate electrical battery model capable of predicting runtime and I-V performance," *IEEE Trans. Energy Convers.*, vol. 21, no. 2, pp. 504–511, Jun. 2006.
- [27] Q. Ouyang, J. Chen, and J. Zheng, "State-of-Charge Observer Design for Batteries With Online Model Parameter Identification: A Robust Approach," *IEEE Trans. Power Electron.*, vol. 35, no. 6, pp. 5820–5831, Jun. 2020.
- [28] P. Chen et al., "Evaluation of Various Offline and Online ECM Parameter Identification Methods of Lithium-Ion Batteries in Underwater Vehicles," *ACS Omega*, vol. 7, no. 34, pp. 30504–30518, Aug. 2022.
- [29] M. Kwak, B. Lkhagvasuren, J. Park, and J.-H. You, "Parameter Identification and SOC Estimation of a Battery Under the Hysteresis Effect," *IEEE Trans. Ind. Electron.*, vol. 67, no. 11, pp. 9758–9767, Nov. 2020.
- [30] J. Han, "From PID to Active Disturbance Rejection Control," *IEEE Trans. Ind. Electron.*, vol. 56, no. 3, pp. 900–906, Mar. 2009.
- [31] Z. Xu, T. Zhang, Y. Bao, H. Zhang, and C. Gerada, "A Nonlinear Extended State Observer for Rotor Position and Speed Estimation for Sensorless IPMSM Drives," *IEEE Trans. Power Electron.*, vol. 35, no. 1, pp. 733–743, Jan. 2020.
- [32] T. Zhang, Z. Xu, and C. Gerada, "A Nonlinear Extended State Observer for Sensorless IPMSM Drives with Optimized Gains," *IEEE Trans. on Ind. Applicat.*, vol. 56, no. 2, pp. 1485–1494, Mar. 2020.
- [33] Y. Feng, F. Bai, C. Xue, and F. Han, "State-of-Charge and State-of-Energy Estimation for Lithium-ion Batteries Using Sliding-Mode Observers," in *2021 40th Chinese Control Conference (CCC)*, Shanghai, China: IEEE, pp. 2382–2385, Jul. 2021.
- [34] L. Zheng, J. Zhu, G. Wang, T. He, and Y. Wei, "Novel methods for estimating lithium-ion battery state of energy and maximum available energy," *Applied Energy*, vol. 178, pp. 1–8, Sep. 2016.
- [35] P. Shrivastava, T. Kok Soon, M. Y. I. Bin Idris, S. Mekhilef, and S. B. R. S. Adnan, "Combined State of Charge and State of Energy Estimation of Lithium-Ion Battery Using Dual Forgetting Factor-Based Adaptive Extended Kalman Filter for Electric Vehicle Applications," *IEEE Trans. Veh. Technol.*, vol. 70, no. 2, pp. 1200–1215, Feb. 2021.
- [36] DATASET- Kollmeyer, Phillip; Naguib, Mina; Skells, Michael (2020), "LG 18650HG2 Li-ion Battery Data", Mendeley Data, V2.
- [37] W. Li, L. Liang, W. Liu, and X. Wu, "State of Charge Estimation of Lithium-Ion Batteries Using a Discrete-Time Nonlinear Observer," *IEEE Trans. Ind. Electron.*, vol. 64, no. 11, pp. 8557–8565, Nov. 2017.